RESEARCH PAPER

Hydrothermal synthesis of nitrogen doped graphene supported cobalt ferrite (NG@$CoFe_2O_4$) as photocatalyst for the methylene blue dye degradation

***Rajinder Singh, Manesh Kumar, Lobzang Tashi, Heena Khajuria, Haq Nawaz Sheikh* ***

Department of Chemistry, University of Jammu, Jammu Tawi, India

ARTICLE INFO

Article History:
Received 8 May 2018
Accepted 4 July 2018
Published 1 August 2018

Keywords:
Cobalt Ferrite
Methylene Blue
Nitrogen Doped Graphene
Photocatalyst
Visible Light

ABSTRACT

A magnetic NG@$CoFe_2O_4$ photocatalyst was developed via a facile hydrothermal method, and subsequently characterized by X-ray powder diffraction (XRD), scanning electron microscopy (SEM), transmission electron microscopy (TEM), Fourier transform infrared spectroscopy (FTIR), and vibrating sample magnetometry (VSM) techniques. The $CoFe_2O_4$ nanoparticles were found to have a size between 100-150 nm and were uniformly dispersed on the nitrogen doped graphene. Magnetic studies showed that the NG@$CoFe_2O_4$ photocatalyst can be easily separated from the solution by a simple bar magnet. The photocatalytic degradation of methylene blue dye (MB) was studied under visible irradiation. The photocatalytic performance of NG@$CoFe_2O_4$ photocatalyst was found to be influenced by structural and optical properties as well as the surface area of the samples. The NG@$CoFe_2O_4$ photocatalyst exhibited improved photodegradation performance when compared with pure $CoFe_2O_4$. The synthesized NG@$CoFe_2O_4$ can be a potential candidate as a visible-light active magnetically separable photocatalyst, so could be used as a potent separation tool in waste water treatment.

How to cite this article
Singh R, Kumar M, Tashi L, Khajuria M, Sheikh HN. Hydrothermal synthesis of nitrogen doped graphene supported cobalt ferrite (NG@$CoFe_2O_4$) as photocatalyst for the methylene blue dye degradation. Nanochem Res, 2018; 3(2):149-159.
DOI: 10.22036/ncr.2018.02.004

INTRODUCTION

About 10000 types of dyes and pigments are synthesized annually worldwide. Approximately 20-30% of the dyes drained from the textiles industry directly into the sea water. Due to the presence of non-biodegradable moieties in the structure and their toxic nature, most of these wastes are harmful for the human health and causes a lot of environmental hazards. So a number of traditional methods like ion exchange, precipitation, coagulation and flocculation, membrane filtration, electrochemical and biological methods have been suggested [1, 2]. To overcome the limitations of standard procedures, oxidative process are applied as an upcoming method for the decomposition of organic wastes. To overcome the limitations of traditional methods, advanced oxidation processes are employed as an upcoming waste management technology for decomposition of organic dyes in polluted water [3–5]. Therefore, the photo-Fenton method is a proficient and economical procedure for handling of wastewater [6–9]. This approach is effective for the generation of extremely reactive, potent oxidant and non-selective reagent hydroxyl radicals (OH) produced due to the photodecomposition of water [1, 5, 8]. The high oxidation potential (2.80) of hydroxyl radicals promote the degradation of non-biodegradable organic pollutants, unsaturated compounds in aqueous medium releasing carbon dioxide, water and other biproducts. [1, 2, 4, 10, 11].

Nowadays material chemists are facing a lot

* Corresponding Author Email: *hnsheikh@rediffmail.com*

of challenges in synthesis of new substances with excellent physicochemical features and various synthetic procedures involved in this technology. Spinel ferrite (MFe_2O_4) magnetic nanocomposites have attracted lots of attention due to their ability to act as the magnetic materials with the excellent chemical stability [12–13]. Applying recycled and external magnetic material facilitate the removal of spinel ferrites magnetic nanocomposites from the treated waste. [14–16]. Cobalt ferrite ($CoFe_2O_4$) magnetic nanocomposites are very potent metal oxides compared to other spinel ferrites, because they have various applications in diverse fields like sensors [17,18], semiconductor photocatalysts [19, 20], biomedical [21], cancer treatment [22], magnetic optical behaviour [23], electrical [24] and antibacterial [25]. It is an extremely stable n-type semiconductor, with a narrow optical band gap (2.0 eV) making it effective even under visible light treatment [26, 13]. So cobalt ferrite magnetic nanocomposite with controlled morphology with desirable physical and chemical properties is considerably significant. Graphene composed of a two-dimensional (2D) sheet of covalently bonded sp^2 carbon atoms, is a structural unit of 3D graphite and 1D carbon nanotubes. The intrinsic strength of this material is predicted to be unmatchable to any other found material [27]. Due to excellent physico-mechanical properties, such as high mobility, optical transparency, quantum Hall effect, mechanical stiffness, etc. graphene and graphene based composite materials are used not only in the micro-, nano-, and opto-electronic industries but also in biotechnological industries [28, 29]. Considering the close relation and controlled interplay of parameters in tuning the performance characteristics of the ferrite materials as photocatalysts, it is thought of investigating $CoFe_2O_4$ particles anchored and dispersed on a heteroatom doped graphene surface. Out of all heteroatom doped graphene arrangements, nitrogen doped graphene (NG) is in the spotlight owing to its intrinsically high electrical conductivity [30, 31]. At the same time, nitrogen doping is observed to be slightly buckling the graphene layers, and this morphological modification can be helpful in anchoring nanoparticles on its surface [32, 33]. Compared to previous studies on Fe_3O_4/graphene and $CoFe_2O_4$/graphene, this material is benefitted from much lower amount and much wider bandwidth that turn NG@$CoFe_2O_4$ to a properly designed catalyst. Considering its simple synthetic method and controllable ratio in the final composites, these kinds of synthesized materials would be highly valuable in commercial use [34, 35]. In this paper, we have synthesized cobalt ferrite anchored on nitrogen doped graphene magnetic nanocomposite via hydrothermal route. This newly synthesized nanocomposite is then and characterized using X-ray diffraction (XRD), scanning electron microscopy (SEM), transmission electron microscopy (TEM), thermogravimetric analysis (TGA), Fourier transform infrared (FT-IR) and UV–visible (UV–vis) spectroscopy. We have also studied the photocatalytic activity of cobalt ferrite magnetic nanoparticles for degradation of MB under visible light irradiation.

EXPERIMENTAL

Materials

Iron acetate, cobalt acetate, potassium permanganate ($KMnO_4$), potassium hydroxide (KOH) and Vulcan carbon (Vulcan XC-72) were procured from Sigma-Aldrich. Phosphoric acid (H_3PO_4), sulfuric acid (H_2SO_4) and ethanol (EtOH) were purchased from Thomas Baker and were used without any further purification.

Synthesis of reduced graphene Oxide (RGO) and nitrogen doped graphene (NG)

Reduced graphene oxide (RGO) was prepared from the graphite powder flakes by modified Hummer's method [36]. Nitrogen-doped graphene (NG) was prepared using RGO. A 60 mL solution (0.5 mg mL^{-1}) of RGO was taken in a round bottom flask and ultrasonicated for 30 min. In this solution 0.5 g of urea was added under vigorous stirring. The solution was then transferred into Teflon-lined autoclave and maintained at 180 °C for 24 h. The NG was collected by filtration, washed with alcohol and distilled water, followed by drying at 80 °C for 12 h.

Synthesis of cobalt ferrite supported nitrogen Doped graphene oxide (NG@$CoFe_2O_4$)

In a typical procedure 50 mg of NG was dispersed in 15 mL of distilled water. The resulting solution was admixed with 50 mg of iron acetate ($Fe(C_2H_3O_2)_2$) and cobalt acetate ($Co(C_2H_3O_2)_2$) in the 2:1 molar ratio. Thereafter the solution was raised to 35 mL by adding absolute ethanol. The resulting solution mixture was stirred at room temperature for 24 h so that Co^{2+} and Fe^{2+} ions are attached to the nitrogen and oxy functional groups

on the graphene framework. The reaction mixture shifted into a 50 mL Teflon lined stainless steel autoclave and maintained at 120°C for 12 h. The resulting solution was filtered followed by washing several times and finally dried at 60 °C. The product obtained is designated as NG@$CoFe_2O_4$. $CoFe_2O_4$ is prepared by the similar procedure for the comparison.

The schematic representation of the synthetic procedure is given in Fig. 1

Photocatalytic test

For exploring photocatalytic activity, 2.5 mg methylene blue (MB) was dissolved in 100 mL of distilled water to form a clear solution. Absorption spectrum of 5 mL of MB dye solution was measured using UV–visible spectrophotometer for recording λ_{max}. As synthesized NG@$CoFe_2O_4$ nanocomposite (1 mg) was mixed with 5 ml MB solution and vigorously stirred in dark for 1 h in order to achieve the adsorption–desorption equilibrium between methylene blue and the as synthesized photocatalyst. Thereafter the mixture was illuminated under the visible light. After exposing the solution solar radiation for 20 min., a 5 mL aliquot was taken from the mixture at different time intervals and absorbance was recorded at λ_{max} = 663 nm. For comparison, the photocatalytic experiment was also conducted in the presence of pure $CoFe_2O_4$.

Spectroscopic and microscopic measurements

The phase purity, crystalline nature and size of the as-synthesized samples were determined from powder X-ray diffraction (PXRD) using D8 X-ray diffractometer (Bruker) at the scanning rate of 12° min^{-1}, with Cu Kα radiation (λ = 0.15405 nm). Transmission electron microscopy (TEM) images were recorded on Tecnai G2 S-Twin transmission electron microscope with field emission gun operating at 200 kV. Samples for TEM measurements were prepared by evaporating a drop of the colloid onto carbon-coated copper grid. The energy spectra were obtained by energy-dispersive X-ray spectrum equipped on a transmission electron microscope. Scanning electron microscopy (SEM) images of the samples were recorded on FEI Nova Nano SEM 450. The infrared spectra were recorded on a Shimadzu Fourier transform infra-red spectrometer (FT-IR) over the range of wave number 4000–400 cm^{-1}, and the standard KBr pellet technique was employed. The magnetic moment as a function of applied field was recorded using vibrating sample magnetometer (VSM), Lakeshore 7410. Thermogravimetric analysis was carried out using a Perkin Elmer SGSA 6000 thermal analyzer with a heating rate of 10 °C min^{-1} under nitrogen atmosphere from room temperature to 900 °C. Light irradiation in photodegradation experiment was carried out using a UV–Visible spectrophotometer (PG

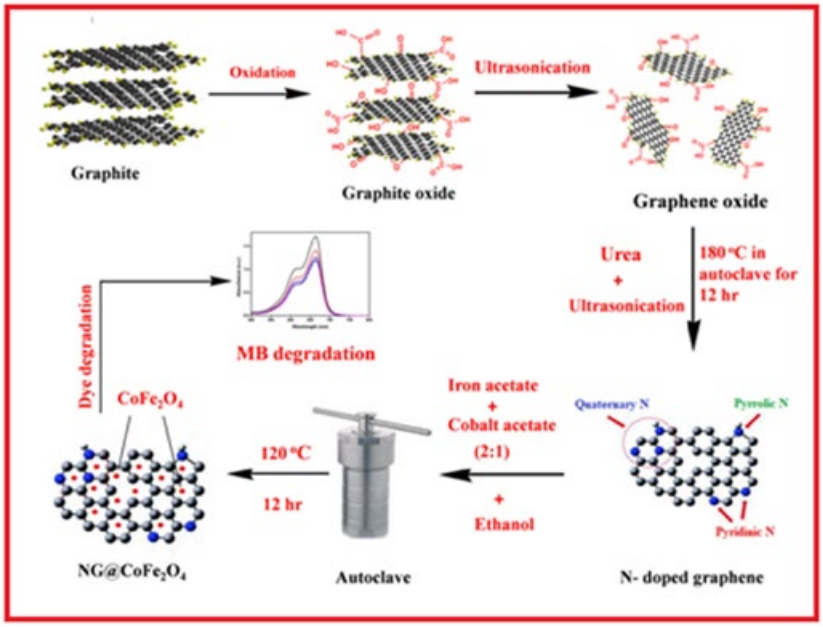

Fig. 1: Schematic representation of the synthetic procedure.

instrumentations, US T-90). All measurements were performed at room temperature.

RESULTS AND DISCUSSION

Crystalline structure and morphology

The structures of the as prepared samples RGO, NG, $CoFe_2O_4$ and NG@$CoFe_2O_4$ were confirmed by PXRD technique. The PXRD results are depicted in Figs. 2 and 3. The X-ray diffraction pattern of RGO shows one characteristic peak (2θ°) at 24.9° (002). The PXRD pattern of NG has a characteristic peak (2θ°) at 24.3° (002). The results obtained for NG are in agreement to literature (JCPDS Card No. 75-1621) [37]. Fig. 3a-b depicts almost all diffraction peaks of the cobalt ferrite nanorods and its nanocomposite with nitrogen doped graphene; $CoFe_2O_4$@NG is indexed to cubic spinel cobalt ferrite (JCPDS No. 00-022-1086). The crystal growth of cobalt ferrite nanorods between the interlayer of NG destroyed the regular layer stacking, leading to weakening the (0 0 2) diffraction peak [38]. The strong and sharp diffraction peaks show highly crystalline nature of $CoFe_2O_4$ and $CoFe_2O_4$@NG nanocomposites.

The average crystallite size of these nanoparticles was calculated using the Scherrer's formula shown in Eq. 1.

$$\beta = \frac{k\lambda}{LCos\Theta} \quad (1)$$

where, L (nm) is the crystallite size, λ (nm) is

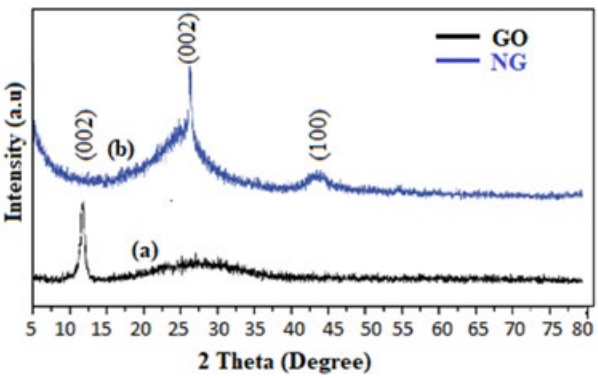

Fig. 2: PXRD pattern of (a) RGO, and (b) NG

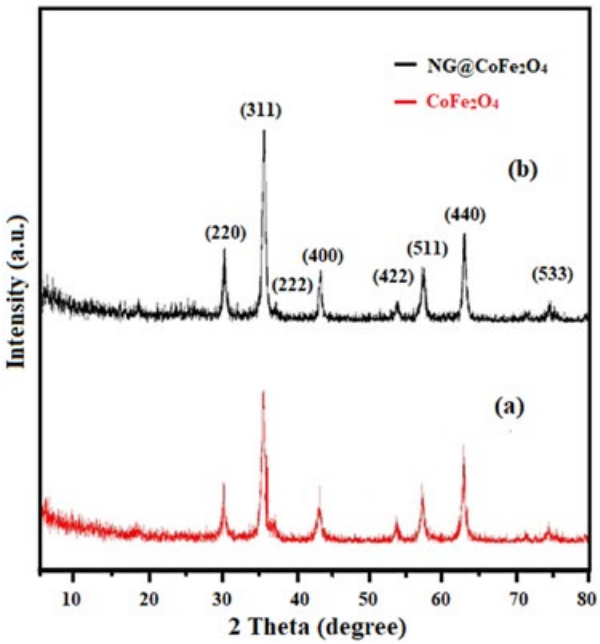

Fig. 3: PXRD pattern of (a) $CoFe_2O_4$ and (b) NG@$CoFe_2O_4$

the wavelength of Cu Kα radiant, λ = 0.15405 nm, β (°) is the full-width at half-maximum (FWHM) of the diffraction peak, θ is the diffraction angle and *K* is the Scherrer constant equal to 0.89. The prominent peaks were used to calculate the average crystallite size of the $CoFe_2O_4$ and $CoFe_2O_4$@NG nanoparticles. The calculated average crystallite sizes of nanoparticles are in the range of 25-40 nm.

Fourier-transform infrared (FT-IR) Characterization

Fig. 4 shows FTIR spectra of the GO, graphene and cobalt ferrite nanorods/graphene composites.

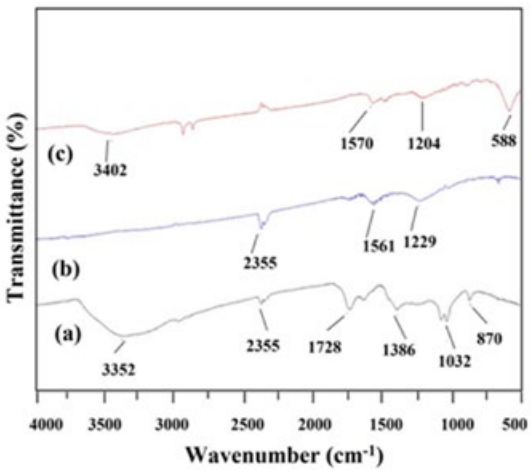

Fig. 4: FT-IR spectrum of (a) GO (b) NG, and (c) NG@ $CoFe_2O_4$

The peaks of GO located at 3353, 1730, 1621, 1386, 1239, 1082 and 1032 cm^{-1} are due to the vibration and deformation bands of O-H, C=O stretching vibrations of carbonyl groups, C=C stretching vibrations of aromatic zone, C-OH stretching vibrations, C-O vibrations from epoxy groups and C-O vibrations from alkoxy groups, respectively [37]. All these band appeared due to the oxygen containing functional groups are not visible in the FTIR spectrum of nitrogen doped graphene (Fig. 4b) possibly due to nitrogen doping and hydrothermal process. The absorption band appeared at 1568 and 1212 cm^{-1} are assigned to skeletal vibration frequencies of the graphene sheets [40-42]. In Fig. 4c there is a slight red shift of the skeletal vibration of graphene sheets for the NG@$CoFe_2O_4$ nanocomposites, which can be explained due to the introduction of $CoFe_2O_4$ into the nitrogen doped graphene framework. Additional band at 589 cm^{-1} in Fig. 4c could be assigned to lattice absorption of Fe-O, confirming the existence of $CoFe_2O_4$ [43].

SEM and TEM analyses

The morphological features of the as synthesized samples were investigated by SEM analysis. Fig. 5a-b depicts the typical SEM images of GO prepared by the modified Hummer's method. The SEM image (Fig. 5a) shows GO sheets have layered structures with uniform surface and wrinkled

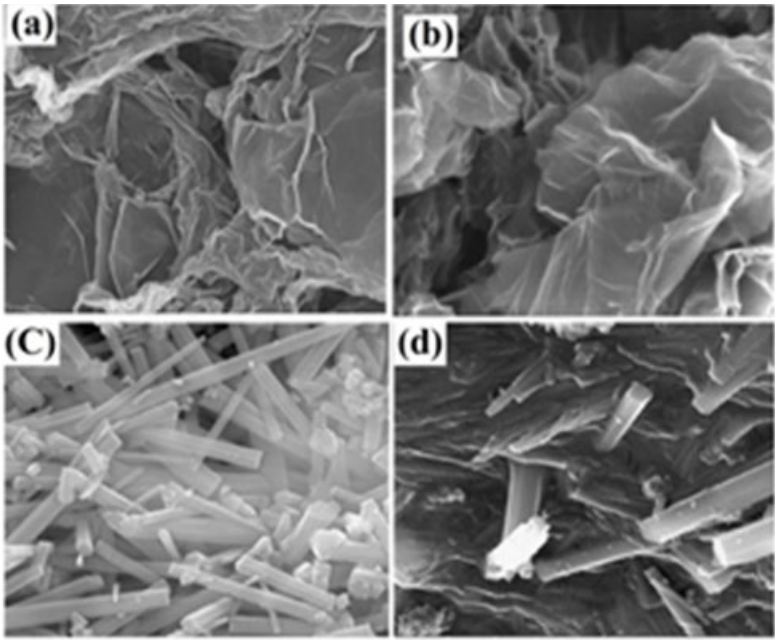

Fig. 5: SEM micrographs of (a) GO (b) NG (c) $CoFe_2O_4$ and (d) NG@$CoFe_2O_4$

from edges. After hydrothermal reduction and doping with the nitrogen an appreciable change in surface morphology takes place as shown in the Fig. 5b. The NG sheets are thinner than GO and the highly wrinkled. The NG sheets are exfoliated and not restacked, that is in accordance to the PXRD results. Fig. 5c shows formation of nano rods of cobalt ferrite structure. In Fig. 5d the distribution of the cobalt ferrite nano rods on the nitrogen doped graphene sheets is clearly visible. Fig. 6a-d show the typical TEM images of GO, NG, $CoFe_2O_4$ and NG@ $CoFe_2O_4$ respectively. Fig. 6a-b reveal the lamellar structure of GO and NG. Fig. 6c-d shows $CoFe_2O_4$ nanotubes and uniformly decorated $CoFe_2O_4$ on the nitrogen doped graphene layers with high density. Notably, the layered structure of NG may support the anchoring of $CoFe_2O_4$ nanotubes on it. The anchoring of $CoFe_2O_4$ also hinders the agglomeration of NG sheets.

Thermal analysis

Fig. 7 shows the TGA graph of NG and NG@ $CoFe_2O_4$ from room temperature to 950 °C at the heating rate of 10 °C min^{-1}. The TGA graphs of nanocomposites NG@$CoFe_2O_4$ (Fig. 7b) displays the hybrid character in its thermal stability as it is

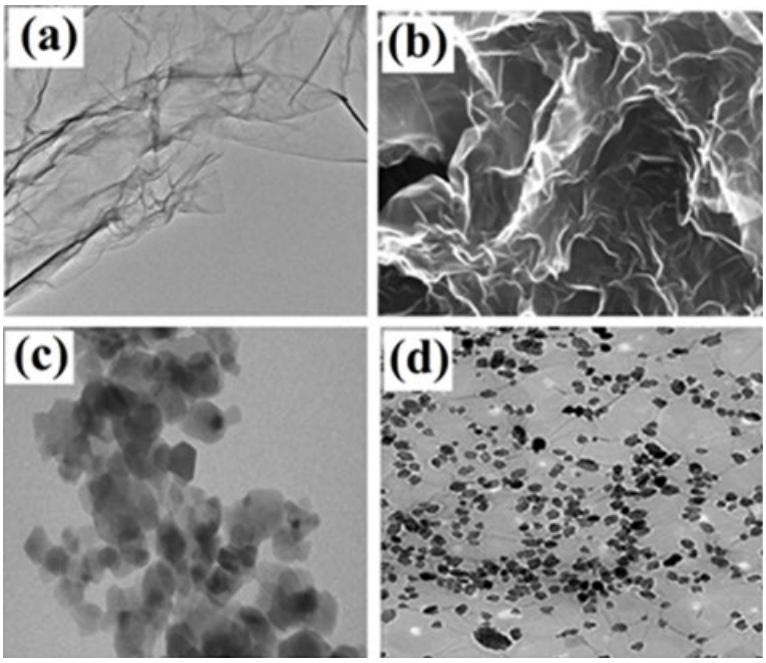

Fig. 6: TEM micrographs of (a) GO, (b) NG, (c) $CoFe_2O_4$ and (d) NG@$CoFe_2O_4$

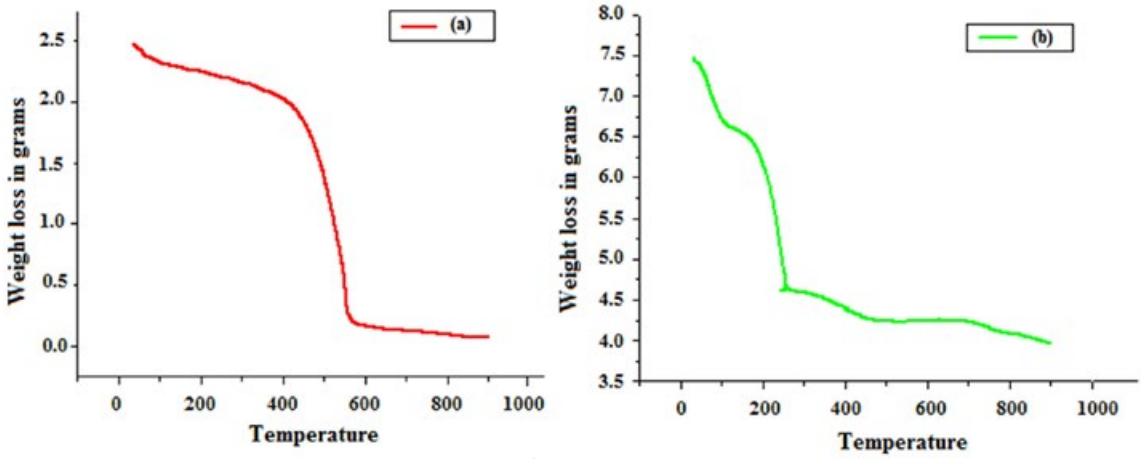

Fig. 7: TGA graphs of (a) NG and (b) NG@$CoFe_2O_4$

more stable than NG (Fig. 7a). The weight loss in case of NG@$CoFe_2O_4$ is less as compared to the NG. The initial rapid weight loss of the composite is possibly due to the portion of nitrogen doped graphene content in the NG@$CoFe_2O_4$ nanocomposite. These measurements show notable quantity of nitrogen doped graphene in nanocomposites.

Magnetic characterisation

Magnetic hysteresis loops of the samples shown in Fig. 8, indicate the strong magnetic nature to a diverging magnetic field. The saturation magnetization of the bare $CoFe_2O_4$ nanorods and NG@$CoFe_2O_4$ composites are 64.2 and 41.5 emu/g, respectively (Fig. 8a-b). The coercivity values are 1062.6 and 493.2 Oe, respectively. The reason for weaker saturation magnetization value of NG@$CoFe_2O_4$ composites is essentially due to the presence of non-magnetic NG in NG@$CoFe_2O_4$. The alteration of the magnetic behaviour due to the presence of NG in $CoFe_2O_4$ indicates that magnetic properties of the hybrid materials could be tuned by adjusting the ratio of ferrite material to NG [44].

Photodegradation of methylene blue (MB)

Methylene blue ($C_{16}H_{18}N_3SCl$) is an important dye used in the textile industries. It is also called as methylthionium chloride. It shows λ_{max} at 662 nm with molar absorption coefficient (ε) 19 $M^{-1}cm^{-1}$ [45]. The photodegradation of MB has been reported in the literature with various metal oxides and metal ferrites such as ZnO [45],

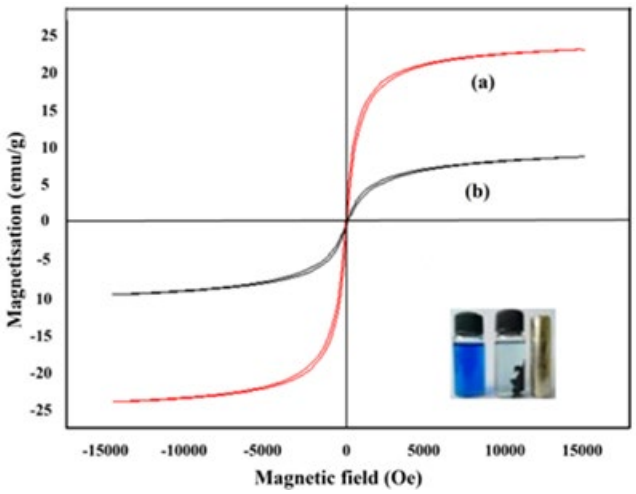

Fig. 8: Magnetic hysteresis loop of (a) $CoFe_2O_4$ and (b) NG@$CoFe_2O_4$

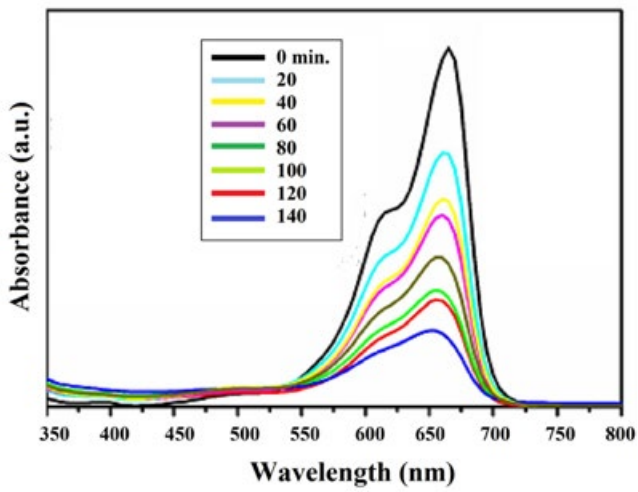

Fig. 9: Absorption spectra of the MB solution taken at different photocatalytic degradation times using NG@$CoFe_2O_4$ as photocatalyst

$MgFe_2O_4$ and MFe_2O_4 (M= Mn, Co) [46, 47]. In order to demonstrate the potential application of the prepared nanocomposite, NG@$CoFe_2O_4$, the photocatalytic experiments were performed on the prepared photocatalyst against MB dye. In the photocatalytic process, the decrease in the value of absorbance for the characteristic absorption peaks (662 nm) as a function of degradation time was monitored. Fig. 9 depicts the UV-Vis absorption spectrum of 5mL of aqueous solution of MB (20 mgL^{-1}) with 5 mg of NG@$CoFe_2O_4$ at an interval of every 20 min. indicating that there is almost a complete degradation of the dye after 140 min. The photodegradation efficiency of NG@$CoFe_2O_4$ was found to be higher than that of bare $CoFe_2O_4$. Fig. 10 depicts the percentage degradation of MB versus exposure time (minutes) in the presence of $CoFe_2O_4$ (*curve b*) and NG@$CoFe_2O_4$ (*curve c*). *Curve c* clearly indicates that the NG@$CoFe_2O_4$ nanocomposite has the excellent photocatalytic activity compared to pure $CoFe_2O_4$ (*curve b*). In Fig. 10, *Curve a* shows the percentage degradation of MB versus time in the absence of photocatalyst.

Recyclability and reusability of the Catalyst (NG@ $CoFe_2O_4$)

The reuse and recycling capabilities of the adsorbents are essential for their functional applications. For a greener and eco-friendly strategy, the reusability of a catalyst is aspired. Through which the process becomes free of waste and also reduces the operational expense of the method. The recycling performance and reusability of as-prepared catalyst (NG@$CoFe_2O_4$) was examined by recycling the catalyst for photodegradation of MB organic azo-dye. The results are depicted in Fig. 11. Such outcome confirm that NG@$CoFe_2O_4$ nanocomposite can be recoverable by magnetic

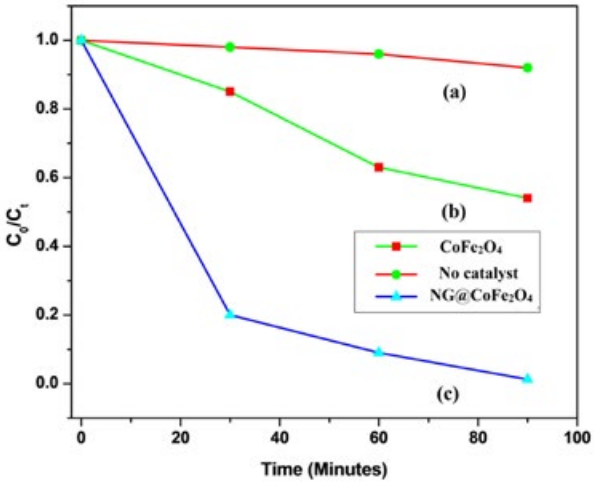

Fig. 10: Kinetics of photodegradation of methylene blue (a) no catalyst (b) $CoFe_2O_4$ and (c) NG@$CoFe_2O_4$ nanocomposites

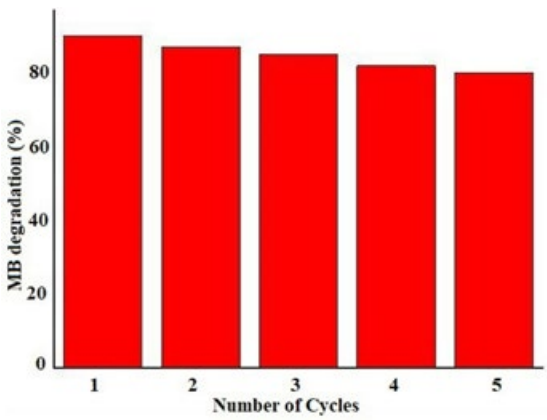

Fig. 11: Removal efficiency of MB on NG@$CoFe_2O_4$ in different catalytic cycles

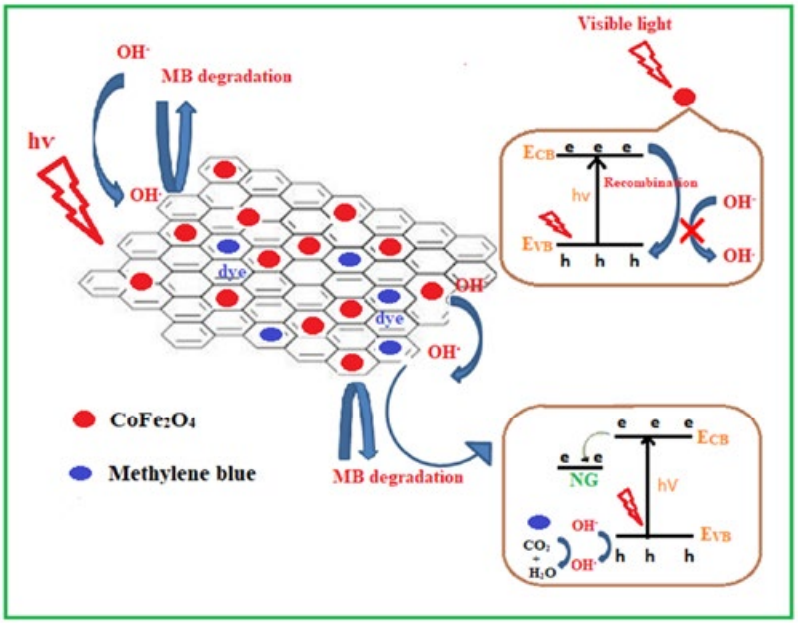

Fig. 12: Plausible mechanism for the photodegradation of MB by NG@$CoFe_2O_4$

separation and reused with little loss in performance during the decolourisation of the dye. It can be seen from the Fig. 11 that there is a small decrease in activity of the catalyst even following five recycles, confirming an excellent stability, recyclability and reusability of NG@$CoFe_2O_4$ photocatalyst. It can be inferred that fast and easy magneto-separable photocatalyst can act as one of the likely materials for treatment of waste water polluted with organic dyes released from dye industries.

Mechanism of MB photodegradation

The notable enhancement of MB dye degradation capability for the NG@$CoFe_2O_4$ nanocomposites was given to the introduction of the NG into the photocatalyst arrangement. The diagrammatic representation of the dye degradation pathway is depicted in Fig. 12. In a typical process, the electrons (e^-) migrate from conduction band (CB) to valence band (VB) by the visible light irradiation. Accordingly the holes (h^+) created in the valence band react with hydroxyl (OH^-) coming from water to form •OH radicals [48]. As formed •OH radicals force to start oxidation degradation of MB. It can be clearly seen in the figure that there is no external charge carrier so in that case the delocalized electrons in the bare $CoFe_2O_4$ could possibly rapidly recombine with the holes produced in the conduction band prior to being captured by OH^- [49, 50], prohibiting the further dye degradation. On the other hand, NG@$CoFe_2O_4$ nanocomposites act as a charge carrier due to the presence of a large number of aromatic structures in nitrogen doped graphene that could effectively confine the delocalized electrons and consequently prevent the recombination of electrons and holes [51]. On the basis of above mentioned factors, the holes in the CB have greater possibility to react with OH− to produce OH• radicals. A much higher dye degradation performance was observed for the NG@$CoFe_2O_4$ nanocomposites. The role of nitrogen doped graphene is given as

a. The adsorption of MB is aided on the surface of NG@$CoFe_2O_4$ due to π−π interaction between aromatic domain of the dye MB and NG sheets.

b. It prevents the electron hole recombination in $CoFe_2O_4$, as it acts as photoelectron acceptor so promoting an effective photocatalytic degradation of MB molecules.

CONCLUSION

In conclusion, we have summarized the structural and magnetic photocatalytic behaviour of $CoFe_2O_4$ and NG@$CoFe_2O_4$ nanocomposites fabricated via hydrothermal method. PXRD results validate the formation of NG@$CoFe_2O_4$ nanocomposites. SEM and TEM micrographs reveal the morphological and topological traits of $CoFe_2O_4$ and NG@$CoFe_2O_4$ nanocomposites. The average crystallite size of amalgamated nanocomposites, calculated

from TEM analysis was found to be in the range of 100-150 nm. The photocatalytic results show that NG@$CoFe_2O_4$ is excellent photocatalyst for photodegradation of MB compared to bare $CoFe_2O_4$. The magnetic nature of this photocatalyst (NG@$CoFe_2O_4$) is also helpful in its easy separation with the help of simple bar magnet.

ACKNOWLEDGEMENTS

We are thankful to UGC New Delhi for funding the research fellowship. We would also like to acknowledge Indian Institute of Technology Mandi and Indian Institute of Technology Guwahati for their technical support. We thank SAIF, Panjab University, Chandigarh for powder X-ray diffraction study.

CONFLICT OF INTEREST

The authors declare that there is no conflict of interests regarding the publication of this manuscript.

REFERENCES

1. Liu L, Zhang G, Wang L, Huang T, Qin L. Highly Active S-Modified ZnFe2O4Heterogeneous Catalyst and Its Photo-Fenton Behavior under UV–Visible Irradiation. Industrial & Engineering Chemistry Research. 2011;50(12):7219-27.
2. Bauer R, Waldner G, Fallmann H, Hager S, Klare M, Krutzler T, et al. The photo-fenton reaction and the TiO_2/UV process for waste water treatment – novel developments. Catalysis Today. 1999; 53(1): 131-44.
3. Houas A, Lachheb H, Ksibi M, Elaloui E, Guillard C, Herrmann J-M. Photocatalytic degradation pathway of methylene blue in water. Applied Catalysis B: Environmental. 2001; 31(2): 145-57.
4. Herney-Ramirez J, Vicente MA, Madeira LM. Heterogeneous photo-Fenton oxidation with pillared clay-based catalysts for wastewater treatment: A review. Applied Catalysis B: Environmental. 2010;98(1-2):10-26.
5. Gajović A, Silva AMT, Segundo RA, Šturm S, Jančar B, Čeh M. Tailoring the phase composition and morphology of Bi-doped goethite–hematite nanostructures and their catalytic activity in the degradation of an actual pesticide using a photo-Fenton-like process. Applied Catalysis B: Environmental. 2011;103(3-4):351-61.
6. Wang Y, Zhao H, Li M, Fan J, Zhao G. Magnetic ordered mesoporous copper ferrite as a heterogeneous Fenton catalyst for the degradation of imidacloprid. Applied Catalysis B: Environmental. 2014;147:534-45.
7. Fallmann H, Krutzler T, Bauer R, Malato S, Blanco J. Applicability of the Photo-Fenton method for treating water containing pesticides. Catalysis Today. 1999;54(2-3):309-19.
8. Andreozzi R, Caprio V, Insola A, Marotta R. Advanced oxidation processes (AOP) for water purification and recovery. Catalysis Today. 1999; 53(1): 51-9.
9. Ghaly MY, Härtel G, Mayer R, Haseneder R. Photochemical oxidation of p -chlorophenol by UV/H 2 O 2 and photo-Fenton process. A comparative study. Waste Management. 2001;21(1):41-7.
10. Liu S-Q, Xiao B, Feng L-R, Zhou S-S, Chen Z-G, Liu C-B, et al. Graphene oxide enhances the Fenton-like photocatalytic activity of nickel ferrite for degradation of dyes under visible light irradiation. Carbon. 2013;64:197-206.
11. Garrido-Ramírez EG, Theng BKG, Mora ML. Clays and oxide minerals as catalysts and nanocatalysts in Fenton-like reactions — A review. Applied Clay Science. 2010;47(3-4):182-92.
12. Maaz K, Mumtaz A, Hasanain SK, Ceylan A. Synthesis and magnetic properties of cobalt ferrite (CoFe2O4) nanoparticles prepared by wet chemical route. Journal of Magnetism and Magnetic Materials. 2007;308(2):289-95.
13. Sun Y, Wang W, Zhang L, Sun S, Gao E. Magnetic ZnFe2O4 octahedra: Synthesis and visible light induced photocatalytic activities. Materials Letters. 2013;98:124-7.
14. Li H, Zhang Y, Wang S, Wu Q, Liu C. Study on nanomagnets supported TiO2 photocatalysts prepared by a sol–gel process in reverse microemulsion combining with solvent-thermal technique. Journal of Hazardous Materials. 2009;169(1-3):1045-53.
15. Yu L, Peng X, Ni F, Li J, Wang D, Luan Z. Arsenite removal from aqueous solutions by γ-Fe2O3–TiO2 magnetic nanoparticles through simultaneous photocatalytic oxidation and adsorption. Journal of Hazardous Materials. 2013;246-247:10-7.
16. Xin T, Ma M, Zhang H, Gu J, Wang S, Liu M, et al. A facile approach for the synthesis of magnetic separable Fe3O4@TiO2, core–shell nanocomposites as highly recyclable photocatalysts. Applied Surface Science. 2014;288:51-9.
17. Zafar Q, Azmer MI, Al-Sehemi AG, Al-Assiri MS, Kalam A, Sulaiman K. Evaluation of humidity sensing properties of TMBHPET thin film embedded with spinel cobalt ferrite nanoparticles. Journal of Nanoparticle Research. 2016;18(7).
18. Paulsen JA, Ring AP, Lo CCH, Snyder JE, Jiles DC. Manganese-substituted cobalt ferrite magnetostrictive materials for magnetic stress sensor applications. Journal of Applied Physics. 2005;97(4):044502.
19. Habibi MH, Parhizkar J. Cobalt ferrite nano-composite coated on glass by Doctor Blade method for photo-catalytic degradation of an azo textile dye Reactive Red 4: XRD, FESEM and DRS investigations. Spectrochimica Acta Part A: Molecular and Biomolecular Spectroscopy. 2015;150:879-85.
20. Alshehri SM, Alhabarah AN, Ahmed J, Naushad M, Ahamad T. An efficient and cost-effective tri-functional electrocatalyst based on cobalt ferrite embedded nitrogen doped carbon. Journal of Colloid and Interface Science. 2018;514:1-9.
21. Pileni MP. Magnetic Fluids: Fabrication, Magnetic Properties, and Organization of Nanocrystals. Advanced Functional Materials. 2001;11(5):323-36.
22. Kim D-H, Nikles DE, Johnson DT, Brazel CS. Heat generation of aqueously dispersed CoFe2O4 nanoparticles as heating agents for magnetically activated drug delivery and hyperthermia. Journal of Magnetism and Magnetic Materials. 2008;320(19):2390-6.
23. Erdem D, Bingham NS, Heiligtag FJ, Pilet N, Warnicke P, Heyderman LJ, et al. CoFe2O4and CoFe2O4-SiO2Nanoparticle Thin Films with Perpendicular Magnetic Anisotropy for Magnetic and Magneto-

Optical Applications. Advanced Functional Materials. 2016;26(12):1954-63.
24. Alshehri SM, Ahmed J, Alhabarah AN, Ahamad T, Ahmad T. Nitrogen-Doped Cobalt Ferrite/Carbon Nanocomposites for Supercapacitor Applications. ChemElectroChem. 2017;4(11):2952-8.
25. Samavati A, F. Ismail A. Antibacterial properties of copper-substituted cobalt ferrite nanoparticles synthesized by co-precipitation method. Particuology. 2017;30:158-63.
26. Casbeer E, Sharma VK, Li X-Z. Synthesis and photocatalytic activity of ferrites under visible light: A review. Separation and Purification Technology. 2012;87:1-14.
27. Akbar F, Kolahdouz M, Larimian S, Radfar B, Radamson HH. Graphene synthesis, characterization and its applications in nanophotonics, nanoelectronics, and nanosensing. Journal of Materials Science: Materials in Electronics. 2015;26(7):4347-79.
28. Balandin AA, Ghosh S, Bao W, Calizo I, Teweldebrhan D, Miao F, et al. Superior Thermal Conductivity of Single-Layer Graphene. Nano Letters. 2008;8(3):902-7.
29. Stoller MD, Park S, Zhu Y, An J, Ruoff RS. Graphene-Based Ultracapacitors. Nano Letters. 2008;8(10):3498-502.
30. Jiao Y, Zheng Y, Jaroniec M, Qiao SZ. Origin of the Electrocatalytic Oxygen Reduction Activity of Graphene-Based Catalysts: A Roadmap to Achieve the Best Performance. Journal of the American Chemical Society. 2014;136(11):4394-403.
31. Qiu Y, Zhang X, Yang S. High performance supercapacitors based on highly conductive nitrogen-doped graphene sheets. Physical Chemistry Chemical Physics. 2011;13(27):12554.
32. Palaniselvam T, Kannan R, Kurungot S. Facile construction of non-precious iron nitride-doped carbon nanofibers as cathode electrocatalysts for proton exchange membrane fuel cells. Chemical Communications. 2011;47(10):2910.
33. Palaniselvam T, Irshad A, Unni B, Kurungot S. Activity Modulated Low Platium Content Oxygen Reduction Electrocatalysts Prepared by Inducing Nano-Order Dislocations on Carbon Nanofiber through N2-Doping. The Journal of Physical Chemistry C. 2012;116(28):14754-63.
34. Ding Y, Liao Q, Liu S, Guo H, Sun Y, Zhang G, et al. Reduced Graphene Oxide Functionalized with Cobalt Ferrite Nanocomposites for Enhanced Efficient and Lightweight Electromagnetic Wave Absorption. Scientific Reports. 2016;6(1).
35. Chang Y-P, Ren C-L, Qu J-C, Chen X-G. Preparation and characterization of Fe3O4/graphene nanocomposite and investigation of its adsorption performance for aniline and p-chloroaniline. Applied Surface Science. 2012;261:504-9.
36. Chen C, Yang Q-H, Yang Y, Lv W, Wen Y, Hou P-X, et al. Self-Assembled Free-Standing Graphite Oxide Membrane. Advanced Materials. 2009;21(29):3007-11.
37. Geng D, Yang S, Zhang Y, Yang J, Liu J, Li R, et al. Nitrogen doping effects on the structure of graphene. Applied Surface Science. 2011;257(21):9193-8.
38. Fu Y, Chen H, Sun X, Wang X. Combination of cobalt ferrite and graphene: High-performance and recyclable visible-light photocatalysis. Applied Catalysis B: Environmental. 2012;111-112:280-7.
39. Murugan AV, Muraliganth T, Manthiram A. Rapid, Facile Microwave-Solvothermal Synthesis of Graphene Nanosheets and Their Polyaniline Nanocomposites for Energy Strorage. Chemistry of Materials. 2009;21(21):5004-6.
40. Jeong H-K, Lee YP, Lahaye RJWE, Park M-H, An KH, Kim IJ, et al. Evidence of Graphitic AB Stacking Order of Graphite Oxides. Journal of the American Chemical Society. 2008;130(4):1362-6.
41. Nethravathi C, Nisha T, Ravishankar N, Shivakumara C, Rajamathi M. Graphene–nanocrystalline metal sulphide composites produced by a one-pot reaction starting from graphite oxide. Carbon. 2009;47(8):2054-9.
42. Bourlinos AB, Gournis D, Petridis D, Szabó T, Szeri A, Dékány I. Graphite Oxide: Chemical Reduction to Graphite and Surface Modification with Primary Aliphatic Amines and Amino Acids. Langmuir. 2003;19(15):6050-5.
43. Cong H-P, He J-J, Lu Y, Yu S-H. Water-Soluble Magnetic-Functionalized Reduced Graphene Oxide Sheets: In situ Synthesis and Magnetic Resonance Imaging Applications. Small. 2010;6(2):169-73.
44. Zhan Y, Meng F, Yang X, Zhao R, Liu X. Solvothermal synthesis and characterization of functionalized graphene sheets (FGSs)/magnetite hybrids. Materials Science and Engineering: B. 2011;176(16):1333-9.
45. Ameen S, Akhtar MS, Kim YS, Yang OB, Shin H-S. Synthesis and characterization of novel poly(1-naphthylamine)/zinc oxide nanocomposites: Application in catalytic degradation of methylene blue dye. Colloid and Polymer Science. 2010;288(16-17):1633-8.
46. Shahid M, Jingling L, Ali Z, Shakir I, Warsi MF, Parveen R, et al. Photocatalytic degradation of methylene blue on magnetically separable MgFe2O4 under visible light irradiation. Materials Chemistry and Physics. 2013;139(2-3):566-71.
47. Liu S-T, Zhang A-B, Yan K-K, Ye Y, Chen X-G. Microwave-enhanced catalytic degradation of methylene blue by porous MFe 2 O 4 (M = Mn, Co) nanocomposites: Pathways and mechanisms. Separation and Purification Technology. 2014;135:35-41.
48. Ahmad M, Ahmed E, Hong ZL, Xu JF, Khalid NR, Elhissi A, et al. A facile one-step approach to synthesizing ZnO/graphene composites for enhanced degradation of methylene blue under visible light. Applied Surface Science. 2013;274:273-81.
49. Dinh C-T, Pham M-H, Seo Y, Kleitz F, Do T-O. Design of multicomponent photocatalysts for hydrogen production under visible light using water-soluble titanate nanodisks. Nanoscale. 2014;6(9):4819-29.
50. Gao Z, Liu N, Wu D, Tao W, Xu F, Jiang K. Graphene–CdS composite, synthesis and enhanced photocatalytic activity. Applied Surface Science. 2012;258(7):2473-8.
51. Sookhakian M, Amin YM, Basirun WJ. Hierarchically ordered macro-mesoporous ZnS microsphere with reduced graphene oxide supporter for a highly efficient photodegradation of methylene blue. Applied Surface Science. 2013;283:668-77.